

ELECTROTHERMALLY ACTUATED FREE SPACE BOARD-TO-BOARD OPTICAL INTERCONNECT WITH ZERO POWER HOLD

J.B. Chou¹, K. Yu¹, D.A. Horsley², S. Mathai³, B. Yoxall², M. Tan³, S.Y. Wang³, and M.C. Wu¹

¹ University of California, Berkeley, California, USA

² University of California, Davis, California, USA

³ HP Labs, Palo Alto, California, USA

ABSTRACT

We present an electrothermally actuated MEMS lens scanner for board-to-board free-space optical interconnect systems capable of zero standby power. U-shaped thermal actuators, brakes, and lens frames are designed, fabricated, and characterized with a vertical cavity surface emitting laser (VCSELs) for dynamic beam steering. We demonstrate up to 170 μm displacement, at a maximum speed of 350 $\mu\text{m}/\text{s}$. The mechanical brakes have a holding force of 1.6 mN with switching speeds of up to 100 Hz. A telecentric (4- f) optical interconnect operating at 1.25 Gb/s is demonstrated. The microlens scanner increases the tilt tolerance of the board by 2.5°.

KEYWORDS

Optical MEMS, Optical interconnect, Electrothermal, actuator, Free space, Bi-stable brake, Stepper motor, Optical beam steering, Free-space optical communication

INTRODUCTION

Free-space optical interconnect using arrays of VCSELs can significantly increase the board-to-board interconnect bandwidth, relieving the bottleneck of traditional backplane-based interconnect systems in computer servers [1]. However, static alignment errors due to board rotation/tilt and insertion offsets have prevented the deployment of such technology. We present a low power adaptive free-space optical interconnect using an electrothermal MEMS lens scanner for beam steering. Once static alignment is obtained, a mechanical bi-stable braking structure holds the lens in place thus dissipating zero power.

Our previous work demonstrates dynamic optical alignment using electrostatic MEMS lens scanners with feedback control [2]. Other prior approaches for MEMS-based optical alignment [3] with feed-forward [4] and feedback control [5] also demonstrate dynamic alignment. This work aims to create a low cost, low power solution for large static misalignments, which infrequently occur in rack mounted server computers due to board insertion variability and tilting. Figure 1 shows the schematic diagram of a board-to-board optical interconnect, with the transmitting board tilt corrected by the MEMS scanner.

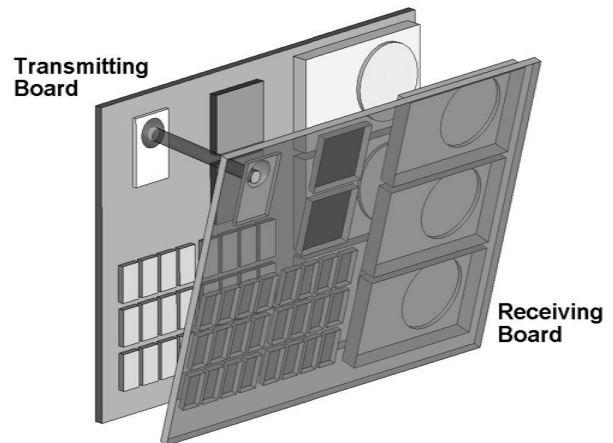


Figure 1: Schematic diagram of the MEMS lens scanner based optical alignment with a tilted receiving board.

OPTICAL DESIGN

Our 4- f optical setup is designed for a board-to-board spacing of approximately 1.8 cm with a transmitting lens ($f_t=6.1$ mm, $D_t=2.8$ mm) and receiving lens ($f_r=3$ mm, $D_r=6$ mm) as shown in Fig. 2(a) [6]. A directly modulated VCSEL with an 850 nm wavelength is located at the back focal plane of the transmitting lens, and a 4 GHz detector with a ~ 60 μm diameter is located at the focal point of the receiving lens. The telecentric optics is insensitive to lateral offsets [6]. As the boards are shifted relative to each other, the incident light is still perpendicular to the receiving lens. Thus, the light is still focused onto the photodetector. The large lens sizes are beneficial to minimize clipping losses and maximize displacement tolerance. Two-dimensional arrays of VCSELs and photodetectors can be used in this optical setup to achieve high data rate (up to Tb/s for 10x10 array).

However, if the two boards are tilted relative to each other, the communication link will be severely degraded, as the optical signal no longer hits the photodetector. Given the transmitting lens focal length of 6.1 mm and max displacement of 170 μm , our lens scanner will theoretically correct a tilt misalignment of up to 1.6°, as shown in Fig. 2(b).

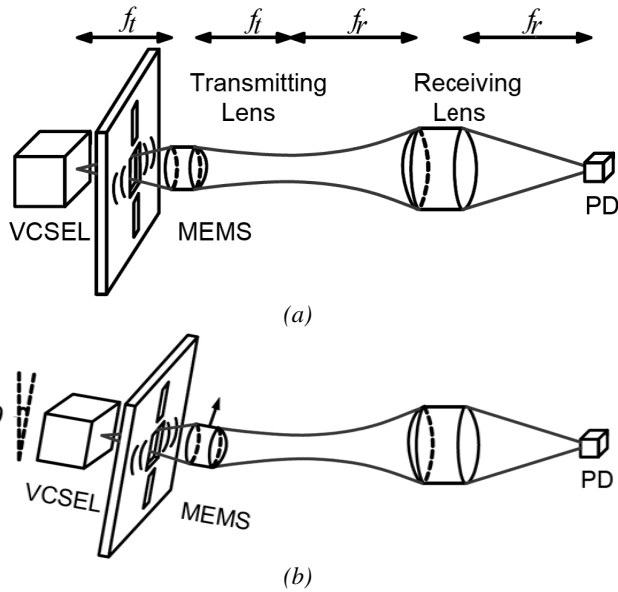


Figure 2: (a) A 4-f optical system without any misalignment. (b) When the transmitting board is tilted, the MEMS scanner steers beam upwards to regain connection.

MEMS DESIGN AND FABRICATION

The full MEMS schematic diagram is shown in Fig. 3. The stepper motor allows for large travel displacements and is only limited by the support springs [7]. The stepper operates by alternating two pairs of thermal actuators for a grip and push motion. U-shaped thermal actuators are chosen for their high force and large displacement characteristics, which are necessary to achieve a large lens scanning distance. To prevent the actuator from slipping upon contact, angled $3 \mu\text{m}$ triangular teeth are etched into the contact areas between the actuators and shuttle.

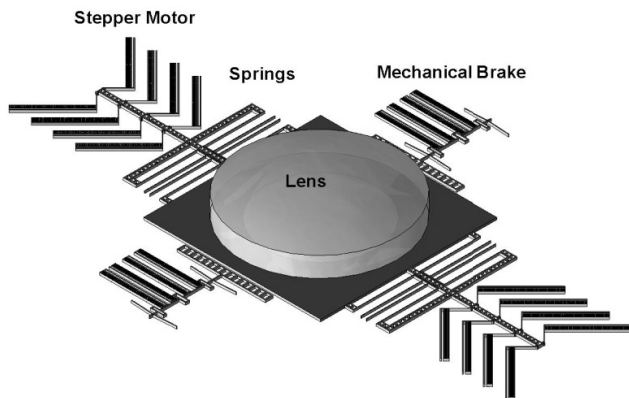


Figure 3: 3D illustration of an electrothermal MEMS scanner with a mounted lens.

A bistable mechanical break is used to clamp and hold the lens frame in place for static displacement offsets, as seen in Fig. 4(b). A curved bistable spring is toggled from one state to another by similar U-shaped actuators as the stepper motor [8]. Because this brake is entirely

mechanical, no power is dissipated when the lens frame is fastened by the brake.

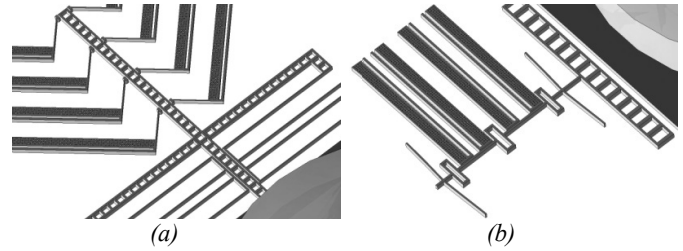


Figure 4: (a) Stepper structure, and (b) Bistable brake

The electrothermal MEMS lens scanner is fabricated by bulk micromachining of 6-inch silicon-on-insulator (SOI) wafer with a $50 \mu\text{m}$ device layer and $2 \mu\text{m}$ thick buried oxide layer. The fabrication steps are shown in Fig. 5. A single front-side mask is used to define the entire device for deep reactive ion etching (DRIE). A through wafer backside etch is used to create an optical path for the VCSEL. Vapor phase hydrofluoric acid (HF) is used to release the device. The lens is directly mounted onto the lens frame using UV curable polymer resin. Scanning electron microscope (SEM) images of the device are shown in Fig. 6.

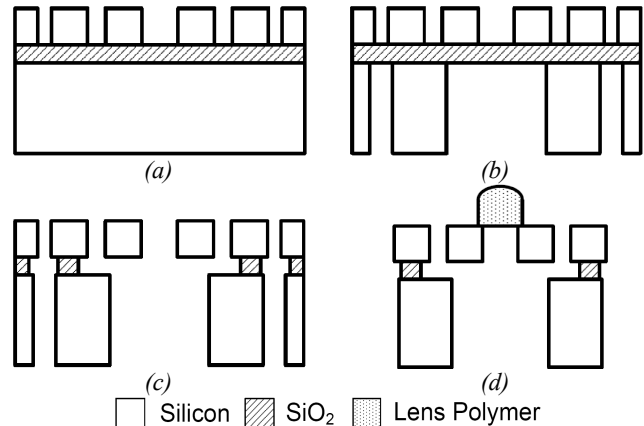


Figure 5: Fabrication steps (a) Front-side silicon etch. (b) Back-side through wafer etch. (c) HF vapor release etch, which also causes automatic dicing, (d) Lens assembly on the MEMS structure.

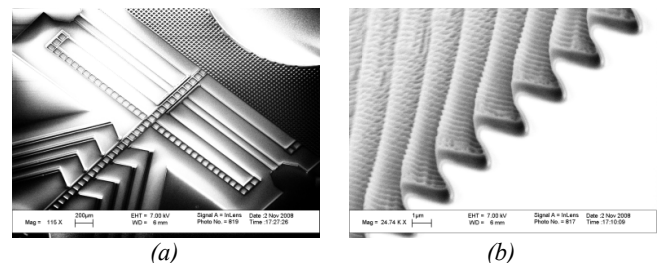


Figure 6: SEM images of (a) the fabricated lens scanner before backside etching, and (b) $3 \mu\text{m}$ -pitch teeth structures to improve friction force between the actuators and the lens shuttle.

MEMS CHARACTERIZATION

Figure 7 shows the lens shuttle position before and after the stepper motor is activated with an operating voltage of 25 V, and a grip-push interval of 10 ms. For reference, the height of each square in the shuttle is 70 μm . Two pairs of thermal actuators displace the shuttle by 170 μm , translating to a maximum pushing force of 1.6 mN. Finite element analysis determines the spring constant to be 9.44 N/m in the up and down direction. Because the net acceleration of the shuttle decreases with increasing displacement, the velocity as a function of displacement is not constant. However, according to video image analysis, the maximum speed is approximately 350 $\mu\text{m/s}$.

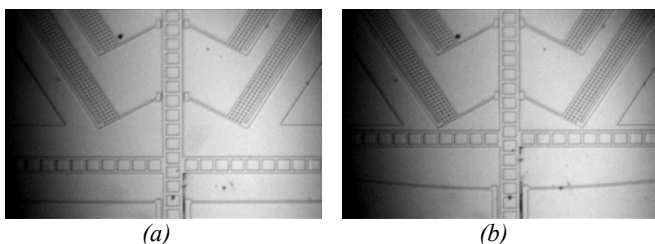


Figure 7: (a) Shuttle at 0 displacement. (b) Shuttle displaced by 170 μm , with a maximum speed of 350 $\mu\text{m/s}$.

The bistable brake operation is shown in Fig. 8, again with an operating voltage of 25 V. Figure 8 shows two thermal actuators pushing the brake to its “open” state to the left (Fig. 8(a)) and “closed” state to the right (Fig. 8(b)). Due to the finite thermal time constant, a maximum switching speed of 100 Hz is observed. Although four pairs of actuators are shown in Fig. 8, only the top two pairs are used.

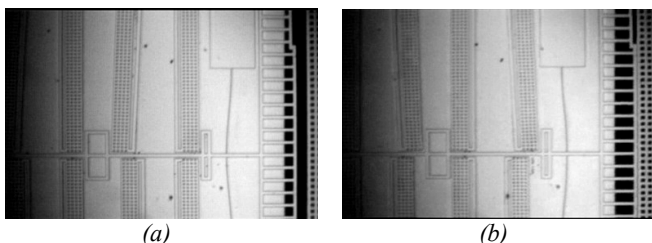


Figure 8: (a) Bistable brake switched to the “open” state by two thermal actuators. (b) Brake switched to the “closed” state, by two different thermal actuators.

The images in Fig. 9 show the stepper motor and brakes functioning together. The shuttle is held and displaced by $\sim 60 \mu\text{m}$ by the stepper motor in Fig. 9(a), and once the brake is released the shuttle falls back to its equilibrium state. Although not shown here, the brakes can hold the shuttle while it is displaced the full 170 μm , translating to a holding force of approximately 1.6 mN. Previous brake systems were fabricated without teeth shown in Fig. 6(b), and resulted in a much lower holding forces. Thus both

the stepper motor and brake system heavily rely on the teeth for enhanced frictional contact.

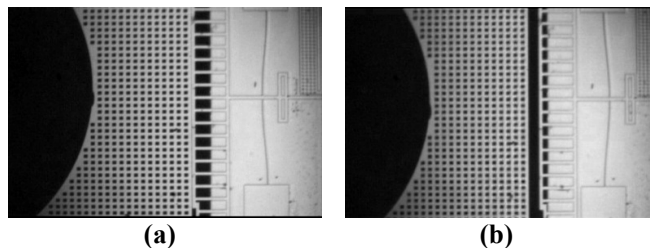


Figure 9: (a) The shuttle is held with a displacement of 60 μm by the stepper actuators. (b) Once the brake is released, the shuttle falls back to its equilibrium state.

EXPERIMENTAL RESULTS

Equation 1 describes the shuttle acceleration as a function of actuator force, spring constant, and mass. Once the lens is mounted on the lens shuttle, the mass of the shuttle is significantly increased, thus resulting in a reduction in acceleration.

$$a_{\text{shuttle}} = \frac{(F_{\text{actuator}} - K_{\text{spring}}x)}{m_{\text{shuttle}}} \quad (1)$$

When the MEMS chip is oriented with the force of gravity pointing downward through the chip, the added mass is believed to cause contact between the shuttle and substrate. As a result, higher actuator forces are needed to displace the shuttle, causing the operating voltage to increase to 30 V in order to observe similar displacements compared to the case without a lens. When the chip is oriented perpendicularly to the earth, such that gravity pulls the shuttle down against the folded springs, we expect the surface friction effect to be diminished, since there is no force pulling the shuttle to the substrate. This is a desired state, as the designed orientation is supposed to be this case, as shown in Fig. 1.

A position sensing detector (PSD) is placed at the imaging plane of the optical setup in order to measure displacement. Figure 10 shows the measured result at different grip and push pulse widths. With shorter pulse width times, the slope of the curve becomes steeper, indicating an increase in velocity. Figure 10 also reveals a stair step displacement pattern which is expected with a grip and push actuation mechanism. The flat signal at the end indicates that the brakes are engaged and thus no movement is detected.

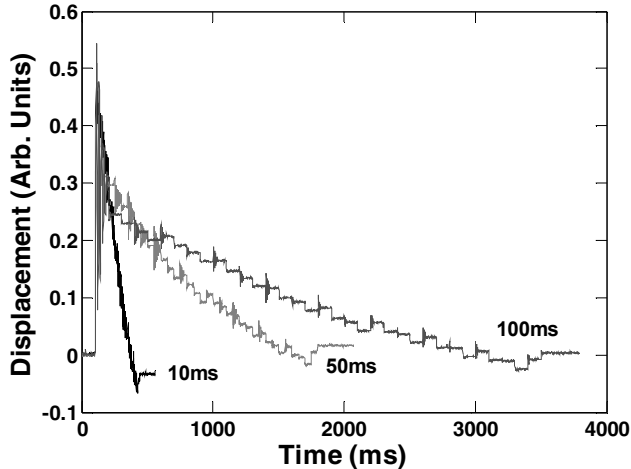


Figure 10: Measured displacement of the MEMS shuttle over time. Different push/grip pulse width times are compared.

To demonstrate active optical alignment we construct a 4-f optical setup with the MEMS lens scanner, as shown in Fig. 11. A 4 GHz high speed photodetector is placed at the imaging plane of the optical setup. When the receiving board is rotate by 5° , we see the eye diagram is closed in Fig. 12(a). However, when we scan the lens up, we regain connection and the eyes become open, as in Fig. 12(b). Due to the large lens diameters and finite detector size, the tilt tolerance without MEMS correction is approximately 2.5° . However, with MEMS enabled, we observe a maximum tolerance of about 5° , thus implying a 2.5° increase in board tilt tolerance.

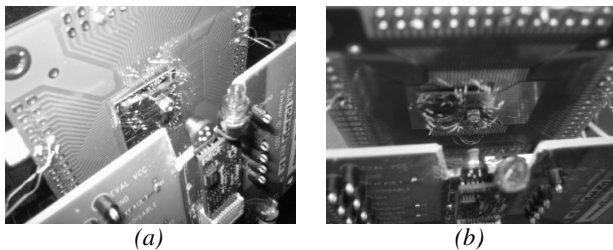


Figure 11: (a) Isometric view of the MEMS (top left) and receiver board (bottom right). (b) Top view of the MEMS (top) and receiver board (bottom). The receiver board is rotated by approximately 5° in both cases.

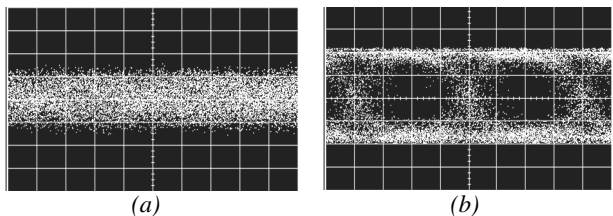


Figure 12: Eye diagrams at 1.25 Gb/s, bandwidth is limited by the VCSEL and can be upgraded to 10 Gb/s with high-speed VCSELs. (a) The closed eye diagram shows the lost optical link during a 5° board rotation. (b) The signal is restored after the MEMS corrects the tilt misalignment.

CONCLUSION

This work demonstrates an electrothermal based lens scanner for adaptive free space board-to-board optical interconnects. The actuators and brakes have been successfully designed, fabricated, and characterized. A maximum travel distance of $170\ \mu\text{m}$ with a maximum speed of $350\ \mu\text{m/s}$ is measured. The bistable brakes are capable of holding the shuttle at any displacement while dissipating zero power during the hold. Optical alignment capabilities have been demonstrated and allow for an increase of 2.5° tilt tolerance. With an array of VCSELs and photodetectors, the total bandwidth can be significantly increased. We believe our device can provide a compact, low cost, and low power solution to adaptive optical steering systems in a number of other interesting applications.

REFERENCES

- [1] E.M. Strzelecka, D.A. Louderback, B.J. Thibeault, G. B. Thompson, K. Bertilsson, and L. A. Coldren, "Parallel free-space optical interconnect based on arrays of vertical-cavity lasers and detectors with monolithic microlenses," *Appl. Optics*, vol. 37, pp. 2811-2821, 1998.
- [2] J.B. Chou, K. Yu, D. Horsley, B. Yoxall, S. Mathai, M.R.T. Tan, S.Y. Wang, M.C. Wu "Robust free space board-to-board optical interconnect with closed loop MEMS tracking," *Applied Physics A*, 2009.
- [3] A. Tuantranont, V. M. Bright, J. Zhang, W. Zhang, J. A. Neff, and Y. C. Lee, "Optical beam steering using MEMS-controllable microlens array," *Sens. Actuators A: Phys.*, vol. 91, pp. 363-372, 2001.
- [4] V. Milanovic and K. Castelino, "Sub-100 μs settling time and low voltage operation for gimbal-less two-axis scanner," in *Proc. the 2004 IEEE/LEOS International Conference on Optical MEMS*, Takamatsu, Japan, 2004.
- [5] J. H. Park, T. Chung, I. H. Park, J. A. Jeon, B. W. Yoo, M. Kim, and Y. K. Kim, "Fast tracking of light source with micromirror and associated feedback circuit," in *Proc. IEEE/LEOS International Conference on Optical MEMS and Nanophotonics*, Taiwan, pp. 59-60, 2007.
- [6] H.P. Kuo, R. Walmsley, L. Kiyama, M. Tan, S.Y. Wang "Telecentric optics for free-space optical link," *Proc. 16th IEEE Symposium on High Performance Interconnects*, pp. 131-136, 2008.
- [7] J.M. Maloney, D.S. Schreiber, D.L. DeVoe "Large-force electrothermal linear micromotors," *J. Micromech. Microeng.*, vol. 14, pp. 226-234, 2003.
- [8] Q. Lin, J.H. Lang, A.H. Slocum, A.C. Weber "A bulk-micromachined bistable relay with U-shaped thermal actuators," *J. Microelectromechanical Systems*, vol. 14, pp. 1099-1109, 2005.